PHOTONICS Research

Review of exceptional point-based sensors

Jan Wiersig

Institut für Physik, Otto-von-Guericke-Universität Magdeburg, Postfach 4120, D-39016 Magdeburg, Germany (jan.wiersig@ovgu.de)

Received 29 April 2020; revised 26 June 2020; accepted 27 June 2020; posted 30 June 2020 (Doc. ID 396115); published 18 August 2020

Exceptional points are spectral singularities in open quantum and wave systems that exhibit a strong spectral response to perturbations. This feature can be exploited for a new generation of sensors. This paper explains the basic mechanism and comprehensively reviews the recent developments. In particular, it highlights the influence of classical noise and fundamental limitations due to quantum noise.

https://doi.org/10.1364/PRJ.396115

1. INTRODUCTION

One of the theorems of quantum mechanics states that physical observables are represented by Hermitian linear operators. This is in particular true for the Hamiltonian $\hat{H}$, which represents the energy and governs the time evolution of a given system via the Schrödinger equation ($\hbar$ is set to unity)

$$i\frac{\mathrm{d}}{\mathrm{d}t}|\psi\rangle = \hat{H}|\psi\rangle. \tag{1}$$

However, for open quantum systems, it can be justified to consider effective Hamiltonians that are non-Hermitian or non-self-adjoint, $\hat{H} \neq \hat{H}^\dagger$ [1–5]. Note that we here do not distinguish between Hermiticity and self-adjointness; for caveats, see Ref. [6]. Non-Hermitian Hamiltonians can also be used for open classical wave systems when a Schrödinger-like equation, as in Eq. (1), holds [7–9]. The non-Hermiticity of the Hamiltonian implies that its eigenvalues, the energy eigenvalues, are in general complex numbers. The negative imaginary part is a decay constant related to a finite spectral linewidth at the resonant energy given by the real part of the eigenvalue. In classical optical systems, where resonant frequencies and modes play the role of energy eigenvalues and eigenstates, non-Hermiticity can enter by absorption, gain, and radiation. A special class of non-Hermitian systems is $\mathcal{PT}$-symmetric systems [8,10–13] which are invariant under a combination of parity ($\mathcal{P}$) and time-reversal ($\mathcal{T}$) operations. Such a system can possess an entirely real eigenvalue spectrum despite being non-Hermitian. Applications of $\mathcal{PT}$ symmetry are reviewed in Refs. [14,15].

If the Hamiltonian is not only non-Hermitian but also non-normal, i.e., $[\hat{H}, \hat{H}^\dagger] \neq 0$, then its (right) eigenstates are mutually nonorthogonal. This nonorthogonality becomes maximal at exceptional points (EPs) in parameter space [16–19], at which the eigenstates of the Hamiltonian fail to provide a basis for the Hilbert space. Approaching an EP of order n (short: EP_n), not only n eigenvalues but also the corresponding n states coalesce. While in earlier stages EPs have been regarded as a mathematical curiosity, their existence has been meanwhile proven in experiments on microwave cavities [20–22], optical microcavities [12,23–26] for light confinement, and other systems. An overview on EPs in optics and photonics can be found in Refs. [27,28].

A crucial difference between EPs and conventional degeneracies, so-called diabolic points (DPs), is the strong response of the eigenvalues to external perturbations. When a DP is subjected to a perturbation of strength ε, then the resulting energy (or frequency) splittings are proportional to ε. As illustrated in Fig. 1, this is in strong contrast to the case of an EP_n where the resulting energy splittings are generically proportional to the nth root of ε [16]. Hence, the absolute values of the splittings in the EP case are parametrically larger, meaning that for sufficiently small perturbations, the splitting is larger than in the DP case for exactly the same perturbation.

The splitting enhancement factor, defined as the ratio of the EP-enhanced splitting and the splitting at a corresponding DP, therefore scales with $\varepsilon^{-(1-1/n)}$ for small ε. Formally, this enhancement factor goes to infinity as $\varepsilon \to 0$. It is this strong enhancement at EPs that can be exploited for sensing applications based on the detection of frequency splittings [29]. Devices based on the detection of frequency splittings at DPs are commonly utilized in microcavity sensors for particle detection [30–32], optical gyroscopes [33,34], weak magnetic field sensors [35], nanomechanical mass sensors [36], and bending curvature sensors [37].

In this review paper, we summarize the recent developments in the field of EP-based sensors. The outline of the paper is as follows. In Section 2, the basic mechanism is explained. Theoretical proposals are discussed in Section 3 and experimental realizations are reviewed in Section 4. Section 5 deals with the influence and classical and quantum noise. Finally, a summary and outlook are given in Section 6.

2. BASIC MECHANISM

We describe EP-based sensors in the formalism established in Refs. [29,38]. For an n-fold degeneracy, the sensor is described

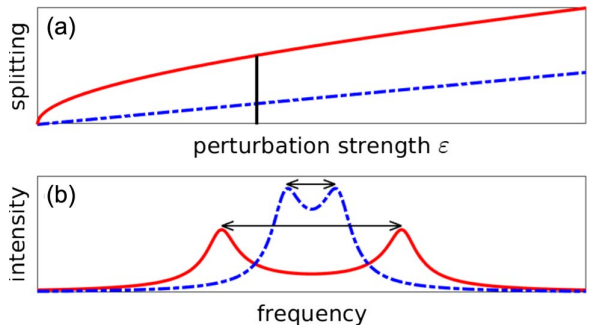

Fig. 1. Illustration of the enhanced frequency splitting induced by perturbing a non-Hermitian Hamiltonian at an exceptional point of second order (red curve) compared to the case of a conventional degeneracy (blue dash-dotted curve). In both cases, the same perturbation has been applied. (a) Splitting versus perturbation strength ε. (b) Spectra for fixed ε designated by the vertical line in (a). The double-arrowed lines indicate the splitting, which is considerably larger for the exceptional point.

by the $n \times n$ system Hamiltonian $\hat{H}_0$, with all eigenvalues being equal. The input quantity of interest is parametrized by ε and is considered as a perturbation

$$\hat{H}(\varepsilon) = \hat{H}_0 + \varepsilon \hat{H}_1, \tag{2}$$

with the $n \times n$ perturbation Hamiltonian $\hat{H}_1$. The resulting eigenvalue splittings are the output quantities which can be measured by spectral means; see the illustration in Fig. 1(b). According to Kato [16], the splittings are proportional to the nth root of ε for an EP_n, whereas for a DP, the splittings are proportional to ε.

For illustration purpose, we focus in this section on sensors based on a two-fold degeneracy. In the case of a DP, the 2×2-matrix $\hat{H}_0$ can be diagonalized to

$$\hat{H}_0|_{\mathrm{DP}} = \begin{pmatrix} E_0 & 0 \\ 0 & E_0 \end{pmatrix}, \tag{3}$$

with complex eigenvalue E_0. Obviously, two linearly independent eigenvectors exist which can be chosen to be $(1,0)^{\mathrm{T}}$ and $(0,1)^{\mathrm{T}}$. The superscript T marks the transpose of the vector. At an EP a diagonalization is not possible, but a transformation to

$$\hat{H}_0|_{\mathrm{EP}} = \begin{pmatrix} E_0 & A_0 \\ 0 & E_0 \end{pmatrix} \tag{4}$$

is with complex eigenvalue E_0 and off-diagonal element $A_0 \neq 0$. By scaling the matrix [Eq. (4)], the off-diagonal element A_0 can be replaced by unity, which would give the Jordan normal form of the EP. In contrast to the matrix in Eq. (3), the matrix in Eq. (4) has only one eigenvector (up to proportionality), $(1,0)^{\mathrm{T}}$.

With the general 2×2 perturbation Hamiltonian

$$\hat{H}_1 = \begin{pmatrix} E_1 & A_1 \\ B_1 & E_2 \end{pmatrix}, \tag{5}$$

it is straightforward to show that the eigenvalue splitting of $\hat{H}$ for the DP is proportional to ε,

$$\Delta E_{\mathrm{DP}} = \varepsilon \sqrt{(E_2 - E_1)^2 + 4A_1B_1}. \tag{6}$$

For the EP, the splitting is

$$\begin{aligned} \Delta E_{\mathrm{EP}} &= \sqrt{\varepsilon}\sqrt{\varepsilon(E_2 - E_1)^2 + 4A_0B_1 + 4\varepsilon A_1B_1} \\ &= \sqrt{\varepsilon}\sqrt{4A_0B_1} + \mathcal{O}(\varepsilon), \end{aligned} \tag{7}$$

which is proportional to $\sqrt{\varepsilon}$ for small $|\varepsilon|$ provided that $B_1 \neq 0$. In this generic case, we can conclude that for sufficiently small perturbation strength, the splitting in the EP case is larger than in the DP case; see Fig. 1(a). The splitting in the EP case strongly depends on $|A_0|$ which, in Ref. [39], is called the strength of the EP and is compared metaphorically to the tension of a crossbow. The larger the tension, the larger the enhancement of the effect of the perturbation, which is the pulling of the trigger. The DP has zero strength ($A_0 = 0$), corresponding to an untensioned crossbow.

Note that for non-Hermitian Hamiltonians, the splittings in Eqs. (6) and (7) are in general complex valued. It is therefore appropriate to measure both the real frequency splitting $\mathrm{Re}\,\Delta E$ and the linewidth splitting $-2\,\mathrm{Im}\,\Delta E$ which can be done; see, for example, Refs. [30,40]. If only the real part of the splitting is experimentally accessible, then one should arrange a situation where the complex splitting is not dominated by the imaginary part.

It is mentioned that the EP enhancement also applies to the individual shift of (the real part of) the frequencies, but not to the mean value of the two frequencies. The measurement of frequency shifts is the more common sensing scheme for microcavity sensors. However, independent of the EP enhancement, one considerable advantage of measuring the splitting is that it is intrinsically self-referenced [30], i.e., there is no need for an external reference to suppress or eliminate thermal drifts, etc.

For passive systems, i.e., systems without gain, at an EP_2 there is an upper bound of the strength of the EP in the Hamiltonian [Eq. (4)] [38] (for caveats see Ref. [41]):

$$|A_0| \leq 2|\mathrm{Im}\,E_0|. \tag{8}$$

As the frequency splitting [Eq. (7)] has to overcome the individual linewidths in order to separate the modes spectrally [Fig. 1(b)] by standard means, one has to come close to this bound [Eq. (8)]. For active systems, including $\mathcal{PT}$-symmetric systems, a bound as in Eq. (8) does not exist. Hence, one can introduce gain to narrow the spectral linewidth, thereby improving the resolvability of the peaks [31,42]. Further methods to efficiently resolve spectral peaks are the interferometric detection of frequency splittings [43] and the harmonic inversion technique [44].

For an EP_3, the Jordan normal form [cf. Eq. (4) with $A_0 = 1$] of the 3×3 system Hamiltonian reads

$$\hat{H}_0|_{\mathrm{EP}} = \begin{pmatrix} E_0 & 1 & 0 \\ 0 & E_0 & 1 \\ 0 & 0 & E_0 \end{pmatrix}. \tag{9}$$

The matrix in Eq. (9) has only one eigenvector $(1,0,0)^{\mathrm{T}}$, again up to proportionality, with complex eigenvalue E_0. This degeneracy is lifted by a generic 3×3 perturbation Hamiltonian $\hat{H}_1$ [as in Eq. (2)], leading to three eigenvalues. For small $|\varepsilon|$, the eigenvalue splittings scale with $\sqrt[3]{\varepsilon}$, which gives an even stronger enhancement than in the EP_2 case.

In the literature, the enhanced eigenvalue splitting has often been called enhanced sensitivity. However, the term "sensitivity" might be misleading [45], as it is used in two different ways: (i) for the transduction coefficient of the sensor from the input quantity of interest (here ε) to the output quantity (here ΔE), or (ii) for the smallest measurable change of the input quantity. The latter is the precision of the sensor, and it is characterized by the signal-to-noise ratio. Because of its ambiguity, the term "sensitivity" is avoided henceforth.

3. THEORETICAL PROPOSALS

There have been a number of proposals for EP-based sensors in various different physical settings; the first was on whispering-gallery microcavities for single- or few-particle detection [29,38]; see Fig. 2(a). Whispering-gallery microcavities confine clockwise (CW) and counterclockwise (CCW) propagating light waves with ultralow losses by total internal reflection; see Refs. [46,47]. Microcavity sensors for label-free particle detection are commonly used; see, Refs. [30,48]. In the context of EP-enhanced sensing, the Hamiltonian in Eq. (4) appears naturally in a two-mode approximation in the basis of CCW and CW propagating waves, with state vector $(\psi_{\mathrm{CCW}}, \psi_{\mathrm{CW}})^{\mathrm{T}}$. The diagonal elements are the frequencies of the waves, which are equal (here E_0), as required by reciprocity [38]. The off-diagonal elements are backscattering coefficients, which can be different due to asymmetric backscattering at deformed boundaries and external or internal scatterers (e.g., air holes) [9,25,38,39,49–52]. At an EP_2, one of the backscattering coefficients is zero, and the other one, here A_0, is nonzero. Physically, this means that there is coherent backscattering from the CW to the CCW propagating direction but not the other way around. The backscattering is said to be fully asymmetric. As a result, only one eigenvector $(1,0)^{\mathrm{T}}$ exists, which corresponds to a purely CCW propagating mode. This unidirectional propagation reflects the chirality of the EP [50,53–55]. A target particle approaching the evanescent field of the microcavity corresponds to the perturbation in Eq. (5); it leads to a square-root frequency splitting as in Eq. (7).

Further approaches to implementing EPs in microdisk cavities with the purpose of enhanced sensing have been introduced by appropriate boundary deformations generating EPs of fourth order [56], and by using a rotationally symmetric layered refractive-index profile [57]. The latter approach has been proposed for sensing the refractive index of a thin additional layer.

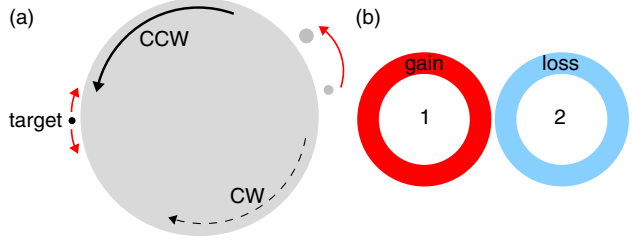

Fig. 2. Two proposals for EP-based sensors. (a) Microdisk cavity with two external scatterers (particles or nano-tips on the right) which implement an EP_2 by generating fully asymmetric backscattering. As a result, only one mode [here counterclockwise (CCW) propagating] of the given mode pair exists. A target particle shown on the left induces additional backscattering, leading to an enhanced frequency splitting. (b) $\mathcal{PT}$-symmetric pair of microrings, one with gain (ring 1) and one with loss (ring 2).

Another scheme is based on coupled cavities [58], as illustrated in Fig. 2(b). Two microrings in close proximity were coupled by their evanescent fields. They are supposed to be identical except that one cavity possesses gain and the other one exactly the same amount of loss. Hence, the system is $\mathcal{PT}$-symmetric. In a two-mode approximation with state vector $(\psi_1, \psi_2)^{\mathrm{T}}$, the Hamiltonian is that of a $\mathcal{PT}$-symmetric dimer

$$\hat{H}_0 = \begin{pmatrix} \omega_0 + i\alpha & g \\ g & \omega_0 - i\alpha \end{pmatrix}. \tag{10}$$

Here, ω_0 is the real-valued frequency, $\alpha \geq 0$ is the gain/loss coefficient, and $g \geq 0$ is the coupling strength. The eigenvalues of the Hamiltonian in Eq. (10) are given by

$$E_{\pm} = \omega_0 \pm \sqrt{g^2 - \alpha^2}. \tag{11}$$

The eigenvalues degenerate if $g = \alpha$. This degeneracy is a DP with eigenvectors $(1,0)^{\mathrm{T}}$ and $(0,1)^{\mathrm{T}}$ if $\alpha = 0$; otherwise, it is an EP with a single eigenvector $(1, -i)^{\mathrm{T}}/\sqrt{2}$. Associated with the latter situation, there is the so-called $\mathcal{PT}$-symmetric phase $g \geq \alpha$, where the eigenvalues are real valued. In the $\mathcal{PT}$-broken phase $g < \alpha$, the eigenvalues are complex conjugate of each other. As in the previous example, the proximity of a target particle is a perturbation to the system Hamiltonian, here in Eq. (10). Assuming that the target particle comes close only to the gain microring, the particle modifies the frequency of the associated mode of the gain ring by an amount ε. This leads to the perturbation Hamiltonian

$$\hat{H}_1 = \begin{pmatrix} 1 & 0 \\ 0 & 0 \end{pmatrix}. \tag{12}$$

The resulting frequency splitting is $\sqrt{i\alpha\varepsilon}$ for $|\varepsilon| \ll 4\alpha$. Here, the real and imaginary splittings are of the same size. Note that the validity of the two-mode approximation [Eq. (10)] is questionable as long-lived modes in optical microrings come in degenerate pairs, with one CW propagating mode and one CCW propagating mode. Hence, a four-mode approximation is more appropriate [59].

A related two-mode $\mathcal{PT}$-symmetric system consisting of two coupled nanobeam cavities has been suggested [60]. A combination with optomechanics for enhanced metrology for displacement measurements has been presented in Ref. [61].

It has been proposed to apply the concept of EP-based sensing also to cavity-based optical gyroscopes [62,63] for the measurement of rotations. Optical gyroscopes are being widely used nowadays for navigation, e.g., in commercial aircraft. The principle of operation is the Sagnac effect. It is the opposite shift of the frequencies of counterpropagating optical waves in a rotating cavity, and scales linearly with the rotational velocity Ω. If the non-rotating system is prepared at an EP_2, then the rotation-induced frequency splitting is proportional to $\sqrt{\Omega}$. For a $\mathcal{PT}$-symmetric pair of coupled microrings such as in Fig. 2(b), it has been shown that the splitting is enhanced when the pair of rings is rotated. Remarkably, in the limit of maximum enhancement, the splitting is independent of the radii of

the rings involved [62]. An improvement of more than six orders of magnitude has been estimated. A single-cavity approach based on a microring with $\mathcal{PT}$-symmetric variation of the refractive index in the azimuthal direction has also been introduced [63]. Yet another approach to EP-enhanced measurements of rotations is to exploit the chirality of EPs [64].

Using a similar Hamiltonian as in Eq. (10), a bilayer structure composed of two different metamaterials with split-ring resonators has been proposed for refractive-index sensing in the terahertz regime [65], and a multi-layer structure based on the resonant optical tunneling effect has been suggested for biosensing [66]. Further proposals have been made for detecting dark-matter candidates [67], non-Newtonian effects in gravitation [68], and gravitational waves [69].

The advantage of the strong response at an EP is a disadvantage for fabrication since low tolerances are required. As a solution to this problem, the so-called exceptional surfaces have been introduced [70,71]. The idea is that certain perturbations do not move the system away from the EP. Examples of such perturbations are changing the values of A_0 and E_0 (equally in both diagonal elements) in the Hamiltonian in Eq. (4). Hence, the values of A_0 and E_0 define a two-parameter family of EPs, the exceptional surface. Provided that the system's response is tailored such that most of the experimental uncertainties shift the operating point along the exceptional surface, the system can be robust and, at the same time, enhanced eigenvalue splittings are possible if the target perturbation pushes the system away from the surface.

An interesting setup for enhanced sensing with EPs of higher order is based on photonic spin–orbit interaction [72]. The spin–orbit interaction couples chiral dipolar modes in different cavities via an adjacent waveguide in a unidirectional manner. This is analogous to the fully asymmetric backscattering of CW and CCW propagating waves in a perturbed whispering-gallery cavity, but the setup can be scaled to higher-order EPs. Note that this setup can be considered as an application of the just-discussed concept of exceptional surfaces. Numerical simulations have shown an $\epsilon^{1/10}$ behavior of the frequency splittings at an EP_{10}. Microwave experiments have demonstrated evidence for unidirectional coupling, but there is no experimental demonstration of the enhanced sensing in this setup.

4. EXPERIMENTAL REALIZATIONS

Based on the original proposal [29], various experimental realizations of EP-based sensors have been developed [73–81]. Figure 3 shows a non-exhaustive compilation.

The first demonstrations of the superior performance of such sensors were done for single-particle detection [73] and thermal sensing [74] (see also Ref. [82]). In Ref. [73] the authors investigated a whispering-gallery microtoroidal cavity

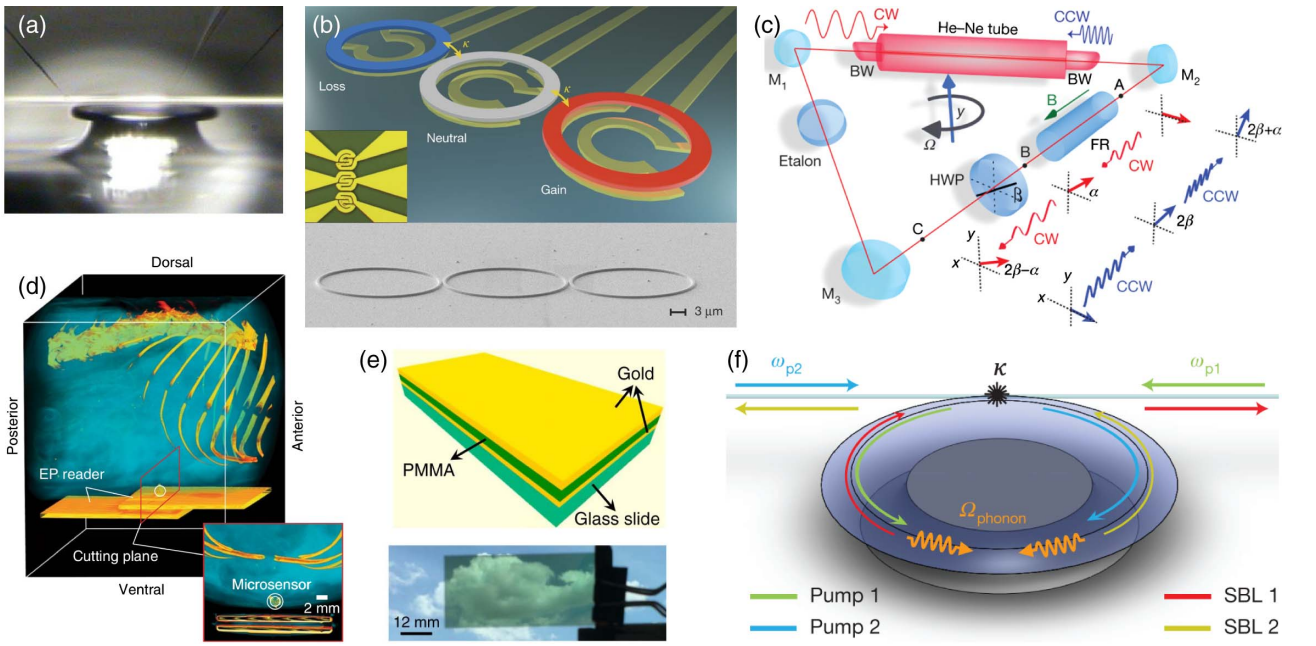

Fig. 3. Various experimental realizations of EP-based sensors. (a) Optical image of a microtoroidal cavity together with a fiber-taper waveguide and three nano-tips for particle detection. Reprinted by permission from Springer Nature: Nature [73], copyright 2017. (b) Illustration and SEM (scanning electron microscope) image of a $\mathcal{PT}$-symmetric ternary microring system for thermal sensing; inset exposes the heating elements underneath each cavity for fine-tuning and thermal perturbation. Reprinted by permission from Springer Nature: Nature [74], copyright 2017. (c) Sketch of a ring laser gyroscope with three mirrors, a Faraday rotator (FR), a half-wave plate (HWP), two Brewster windows (BW), and a He–Ne gas tube as gain medium. Reprinted by permission from Springer Nature: Nature [80], copyright 2019. (d) Computed tomography reconstruction of a wireless $\mathcal{PT}$-symmetric microsensor implanted in a rat abdomen. Reprinted by permission from Springer Nature: Nature Electronics [78], copyright 2019. (e) Schematics and optical image of the thermo-sensitive microscope slide for thermal mapping; from Ref. [75]. (f) Illustration of a laser gyroscope with stimulated Brillouin laser (SBL) action pumped optically at two different frequencies ω_{p1} and ω_{p2} via an attached waveguide which induces backscattering with rate κ. Reprinted by permission from Springer Nature: Nature [81], copyright 2019.

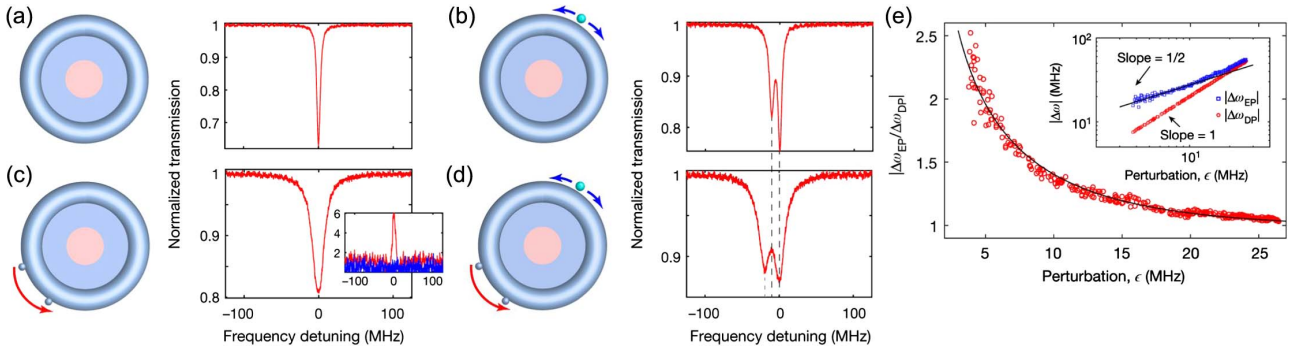

Fig. 4. Results on the microtoroidal sensor in the experiment of Chen *et al.* [73]. The transmission spectra of a DP-based sensor (a) before and (b) after adsorption of a target particle on the surface of the cavity. The transmission spectra of an EP-based sensor (c) before and after (d) adsorption of the same target particle. The blue arrows illustrate the symmetric backscattering at the target particle, and the red arrow marks the fully asymmetric backscattering related to the EP. The dashed vertical lines in (b) and (d) pinpoint the resulting frequency splitting. (e) Measured splitting enhancement factor versus perturbation strength ε. The double logarithmic plot in the inset displays the two different splittings versus ε. The DP-based sensor (red circles) exhibits a slope of 1, whereas the EP-based sensor (blue squares) exhibits a slope of 1/2 (solid black line) for sufficiently small perturbations, confirming the square-root behavior at an EP_2. Reprinted by permission from Springer Nature: Nature [73], copyright 2017.

made of silica. The EP_2 is based on asymmetric backscattering established by two precisely adjusted nano-tips [see Fig. 3(a)], following closely the proposal in Ref. [29]; see Fig. 2(a). Figure 4 embodies the central result of Ref. [73]. In the absence of a target particle the transmission spectra for the DP-based sensor [Fig. 4(a)] and EP-based sensor [Fig. 4(c)], obtained by coupling light in and out via two waveguides, show no frequency splitting. If the target particle [an (additional) nano-tip or a single polystyrene nanoparticle with a radius of 200 nm] is approaching the cavity a clear splitting can be seen, which is by a factor of around 2 larger in the EP case; cf. Figs. 4(b) and 4(d). Varying the distance between the target particle and the surface of the microtoroid, the splitting enhancement factor as a function of the perturbation strength has been determined [Fig. 4(e)]. Both the real and imaginary parts of the frequency splitting have been measured. A moderate enhancement factor of maximal 2.5 can be observed for small perturbations. Moreover, it has been demonstrated that the resolvability of the splittings at the EP can be improved by optical gain generated by pumping erbium ions embedded into the microcavity.

Figure 3(b) shows the $\mathcal{PT}$-symmetric ternary microring system for thermal sensing [74]. The side cavities experience balanced gain ($i\alpha$) and loss ($-i\alpha$), whereas the middle one is neutral. The desired gain/loss distribution is realized by an inhomogeneous optical pumping of InGaAsP quantum wells inside the microrings. The individual frequencies of the cavities are fine-tuned to the same value using three gold microheaters underneath each cavity. Within a three-mode approximation and a rotating frame, the system Hamiltonian is

$$\hat{H}_0 = \begin{pmatrix} i\alpha & \kappa & 0 \\ \kappa & 0 & \kappa \\ 0 & \kappa & -i\alpha \end{pmatrix}. \tag{13}$$

Adjusting the coupling constant κ to be $\alpha/\sqrt{2}$, an EP_3 is generated. To check the performance for thermal sensing, one of the microheaters has been used to introduce a thermal perturbation of strength ε to the gain cavity,

$$\hat{H}_1 = \begin{pmatrix} 1 & 0 & 0 \\ 0 & 0 & 0 \\ 0 & 0 & 0 \end{pmatrix}. \tag{14}$$

A six-mode approximation is not necessary, as the perturbation acts equally on CW and CCW propagation ring modes. The experiment has clearly demonstrated (real-valued) frequency splittings proportional to $\varepsilon^{1/3}$, with an impressive maximal enhancement factor of 23. The imaginary splittings are strongly influenced by nonlinear gain saturation and laser dynamics, which can be anticipated from the fact that one of the frequencies of the linear system resulting from Eqs. (13) and (14) has a positive imaginary part. These nonlinear dynamic aspects have not been studied in the theory.

The concept of EP-based sensing has also been applied in a modified fashion to thermal mapping [75]. Zhao and coworkers coated a conventional microscope slide such that the corresponding scattering matrix is at an EP_2; note that the definition of an EP of a scattering matrix is ambiguous [83]. Figure 3(e) shows the three-layer structure with a polymer (PMMA) layer sandwiched between two gold films deposited on a silica glass slide. The key idea is that ambient thermal perturbations lead to a local change of the thickness of the polymer layer, causing a strong response of the eigenvalues of the scattering matrix and consequently a drastic increase of the reflection. Through reflection measurements, the temperature distribution of the glass slide can be monitored with a roughly tenfold enhanced optical-thermal signal transduction and high spatial resolution.

Another interesting and potentially very relevant class of realizations is wireless EP-based sensors [76–79]. Applications of wireless sensors range from medical diagnosis to industrial and environmental monitoring. The principle of operation is the inductive coupling between the sensor and a reader. The quantity to be measured detunes capacitive or inductive elements of the sensor, which lead to frequency shifts measured externally by the reader. A particular fascinating experiment, depicted in Fig. 3(d), is on an EP_2-based microsensor subcutaneously implanted in a rat abdomen [78].

The sensor can continuously and accurately track the rat's breathing rate arising from the motion of the abdomen during respiration, which causes a modulation of the inductive coupling between the reader and the sensor. A splitting enhancement factor of 3.2 beyond the DP case limit that applies to all existing wireless readout schemes has been observed. The overall detection limit has been in total lowered by a factor of 26, including the help of the narrowing of spectral lines by the reader's gain. A conceptional difference from previous wireless EP-sensors is here that the reader is a $\mathcal{PT}$-symmetric two-mode system (frequency ω_0, gain/loss coefficient α, and coupling constant g) locked to an EP_2 ($g = \alpha$), and the sensor is an additional single-mode system (frequency ω_s and decay rate γ_s) whose sole function is to generate the perturbation of strength ε by the inductive coupling to the reader,

$$\hat{H}_0 = \begin{pmatrix} \omega_0 + i\alpha & g & 0 \\ g & \omega_0 - i\alpha & 0 \\ 0 & 0 & \omega_s - i\gamma_s \end{pmatrix}, \quad \hat{H}_1 = \begin{pmatrix} 0 & 0 & 1 \\ 0 & 0 & 1 \\ 1 & 1 & 0 \end{pmatrix}. \tag{15}$$

In previous wireless EP-sensors [76,77], the reader and sensor together form a $\mathcal{PT}$-symmetric two-mode system biased at an EP_2, and the perturbation acts on the sensor mode. The new design of Ref. [78] shows a significantly improved performance. A passive wireless sensing system at an EP_3 has been fabricated as well [79].

Ring laser gyroscopes with EP-based enhancement have also been successfully built and investigated [80,81]. Figure 3(c) illustrates the setup of Ref. [80]. It is a macroscopic equilateral cavity made of three highly reflective mirrors. A Faraday rotator, a half-wave plate, and two Brewster windows incorporated on both ends of a He–Ne gas tube are used to establish different gain/loss coefficients γ_1 and γ_2 for CCW and CW propagating waves. In addition, a weak conservative backscattering of counterpropagating waves is introduced by inserting an etalon into the cavity. With g being the strength of the backscattering and ω_0 the frequency of both propagating waves, the Hamiltonian can be written in a two-mode approximation as

$$\hat{H}_0 = \begin{pmatrix} \omega_0 - i\gamma_1 & g \\ g & \omega_0 - i\gamma_2 \end{pmatrix} \tag{16}$$

in the basis of the pair of counterpropagating waves. The system has been biased at the EP_2 with $g = |\gamma_1 - \gamma_2|/2 > 0$ by fine-tuning the differential gain/loss $|\gamma_1 - \gamma_2|$. Rotating the cavity with velocity Ω acts as a perturbation Hamiltonian

$$\hat{H}_1 = \begin{pmatrix} 1 & 0 \\ 0 & -1 \end{pmatrix} \tag{17}$$

with perturbation strength $\varepsilon \propto \Omega$. The resulting frequency splitting is proportional to $\sqrt{\Omega}$. The measured data [80] have clearly demonstrated this enhanced response of the gyroscope at the EP with an enhancement factor larger than 1 order of magnitude.

The laser gyroscope in Ref. [81] is of a very different type. The microscopic system is made of a high-quality silica microdisk; see Fig. 3(f). Stimulated Brillouin processes lead to lasing action of a chosen pair of counterpropagating waves, resulting in ultranarrow spectral linewidths. Moreover, the Brillouin processes modify the frequencies of the two involved modes ω_1 and ω_2 such that they exhibit a nonzero detuning even in the absence of rotation. This detuning can be precisely adjusted by properly choosing the pump frequencies ω_{p1} and ω_{p2}. The presence of the waveguide that is used to pump the Brillouin laser modes induces scattering losses with the rate γ and backscattering of the counterpropagating waves with the rate κ. Assuming dissipative backscattering, only the system Hamiltonian is given by

$$\hat{H}_0 = \begin{pmatrix} \omega_1 - i\gamma & i\kappa \\ i\kappa & \omega_2 - i\gamma \end{pmatrix} \tag{18}$$

in the basis of the pair of counterpropagating waves. Adjusting the pump frequencies such that $|\omega_2 - \omega_1| = 2\kappa > 0$ brings the sensor to an EP_2. Rotating the cavity with velocity Ω acts as the perturbation Hamiltonian in Eq. (17) with strength $\varepsilon \propto \Omega$. The induced frequency splitting is again proportional to $\sqrt{\Omega}$. The experiment in Ref. [81] has confirmed this enhanced response of the gyroscope and reported a splitting enhancement factor of 4.

Recently, EP-based sensors have also been produced in the plasmonic domain [84]. Plasmonic systems are of particular interest for sensing, as electromagnetic fields can be greatly enhanced inside plasmonic hot spots. This opens the possibility to carry out sensing on the nanoscale. The EP-based sensor in Ref. [84] consists of a bilayer structure made of two arrays of dissimilar plasmonic resonators. A Hamiltonian is not provided, as the system has been discussed in terms of second-order differential equations for coupled oscillators. By functionalizing the surface of the sensor, the authors have successfully demonstrated that the sensor can selectively detect anti-immunoglobulin G, an important immunoglobulin in human serum, with enhanced frequency splitting.

5. INFLUENCE OF NOISE

A. Classical Noise

The strong response of EPs to weak perturbations naturally raises the question of the influence of noise on the performance of EP-based sensors. Here we review the work done on classical, i.e., technical, noise related to EP-based sensors. Let us consider the total Hamiltonian with parametric noise

$$\hat{H}_{\text{tot}}(t) = \hat{H}(\varepsilon) + \sum_{j=1}^{K} \xi_j(t) \hat{H}_{\text{noise},j}, \tag{19}$$

where $K \geq 1$ is the number of statistically independent noise sources and the ξ_j are real-valued fluctuations with zero mean $\overline{\xi_j(t)} = 0$. The overline denotes an ensemble average over all possible realizations of the noise. As before, $\hat{H}(\varepsilon)$ is the time-independent and non-Hermitian Hamiltonian describing the sensor and perturbation by virtue of Eq. (2). $\hat{H}_{\text{noise},j}$ are time-independent and in general non-Hermitian operators describing the fluctuations of the matrix elements of the total Hamiltonian. Note that the noise in the total Hamiltonian in Eq. (19) enters the sensor as multiplicative noise in the Schrödinger equation [Eq. (1)]. It describes a noisy EP rather

than a noisy input channel. The latter is relevant for the quantum noise discussed in Section 5.B.

We may classify the noise according to the correlation time. Infinite correlation time implies static disorder which has been studied in Ref. [85]. Not unexpectedly, static disorder blurs the spectral features after ensemble average. Fluctuations with limited correlation time, i.e., temporal noise, have been investigated in Refs. [86–88].

The authors in Ref. [86] have addressed the impact of a single noise source ($K = 1$) on an EP-based sensor made of the $\mathcal{PT}$-symmetric dimer in Eq. (10). The noisy element is a fluctuating on-site frequency detuning described by the noise Hamiltonian

$$\hat{H}_{\mathrm{noise},1} = \begin{pmatrix} 1 & 0 \\ 0 & -1 \end{pmatrix}. \tag{20}$$

The spectrum of $\xi_1(t)$ has been required to be nonwhite, as it has a high-frequency cutoff and a gap around the frequency of the EP. The latter has been justified by the presence of an active stabilization circuit. It is difficult to judge to what extent the various approximations involved are fully consistent. The basic finding of Ref. [86] is that the system is dynamically unstable. Numerics show that the norm of any initial state grows asymptotically like $\exp(\sqrt{2\gamma}t - 1)$ with a fitting constant γ. Nonlinear effects, which might counteract the instability, are ignored.

The general case of K noise sources is treated in Ref. [88]. It is assumed that the ξ_j describe stationary white Gaussian noise $\overline{\xi_i(t)\xi_j(t')} = \gamma_j\delta_{ij}\delta(t - t')$ with noise strengths γ_j. For monochromatic excitation with frequency ω, the dynamics of the density operator $\hat{\rho}(t) = \overline{|\psi(t)\rangle\langle\psi(t)|}$ is described by an inhomogeneous Lindblad-type master equation

$$\frac{\mathrm{d}\hat{\rho}}{\mathrm{d}t} = \mathcal{L}\hat{\rho} + \hat{P}(\omega) \tag{21}$$

with the superoperator $\mathcal{L}$:

$$\mathcal{L}\hat{\rho} = -i(\hat{H}_{\mathrm{eff}}\hat{\rho} - \hat{\rho}\hat{H}_{\mathrm{eff}}^{\dagger}) + \sum_j \gamma_j \hat{H}_{\mathrm{noise},j}\hat{\rho}\hat{H}_{\mathrm{noise},j}^{\dagger}, \tag{22}$$

and the effective Hamiltonian

$$\hat{H}_{\mathrm{eff}}(\varepsilon) = \hat{H}(\varepsilon) - \frac{i}{2}\sum_j \gamma_j \hat{H}_{\mathrm{noise},j}^2. \tag{23}$$

The pump operator $\hat{P}(\omega)$ in Eq. (21) has poles at the eigenvalues of $\hat{H}_{\mathrm{eff}}$. From the preceding equations it can be concluded that (i) the resolvability of frequency splittings at and near an EP is determined by $\hat{H}_{\mathrm{eff}}$, and (ii) the stability of the system is determined by the superoperator $\mathcal{L}$. The latter can be discussed in Liouville space, where $\hat{\rho}$ and $\hat{P}$ are represented as n^2-dimensional vectors and $\mathcal{L}$ is represented as an $n^2 \times n^2$ matrix (the Liouvillian). A stationary state $\hat{\rho}$ is in general only possible if all eigenvalues of the Liouvillian λ_l have nonpositive real part. A crucial result is that for a noiseless sensor, the Hamiltonian EP_n carries over to a Liouvillian EP_{2n-1} [88,89], i.e., the latter is of higher order than the Hamiltonian one. Hence, the eigenvalues λ_l show an extreme response to noise, so one eigenvalue may easily cross the imaginary axis leading to a dynamical instability.

The instability, however, can be removed by a uniform damping of the sensor, i.e., by adding $-i\kappa\mathbb{1}$ to $\hat{H}_0$, with the rate κ above the critical rate $\kappa_c = \mathrm{Re}\,\lambda_1/2$, with $\lambda_1(\gamma_1, \ldots, \gamma_K)$ being the eigenvalue with the largest real part. Obviously, this reduces the resolvability because the linewidths broaden significantly. Hence, for EP-based sensors operating at or close to the real frequency axis, as for instance in the case of $\mathcal{PT}$-symmetric systems, even small noise can indirectly, via the necessary stabilization, spoil the resolvability.

However, this does not mean that EP-based sensors are fundamentally limited by classical/technical noise. In principle, classical noise can be made arbitrarily small. For instance, it has been demonstrated theoretically for a class of electronic circuits that the extra technical noise originating from the gain in $\mathcal{PT}$-symmetric arrangements can be made negligibly small [87].

B. Quantum Noise

In contrast to classical noise, quantum noise may fundamentally limit EP-based sensing. All existing theoretical approaches [45,90–92] assume the so-called weak dispersive limit, where frequency shifts are much smaller than the spectral linewidths. It is worth emphasizing that none of the experiments reviewed in Section 4 are restricted to this regime. In the theoretical approaches, it is argued that the frequency splitting is not directly measured; instead, it is constructed from field measurements (sampled at various frequencies). Hence, quantum noise limits apply to the field rather than to frequency splittings. The authors in Ref. [45] have shown with elementary calculations based on the Schrödinger equation [Eq. (1)] that the field changes in lowest order are proportional to ε both for DPs and EPs. Hence, the response at the EP is not parametrically larger than at a DP (in absolute values, the response at the EP can be still larger [93]). Without performing any quantum-noise calculations, one can conclude that EP-based sensors do not have a superior scaling behavior in terms of the quantum-limited signal-to-noise ratio.

The full quantum calculations in Refs. [90–92] are based on Heisenberg–Langevin equations

$$i\frac{\mathrm{d}}{\mathrm{d}t}\begin{pmatrix} \hat{a}_1 \\ \vdots \\ \hat{a}_n \end{pmatrix} = \hat{H}(\varepsilon)\begin{pmatrix} \hat{a}_1 \\ \vdots \\ \hat{a}_n \end{pmatrix} + \text{driving} + \text{bath coupling}. \tag{24}$$

The operator $\hat{a}_j$ is a bosonic annihilation operator for the jth mode in the second-quantization formalism. Noise enters additively via stochastic Langevin terms describing the driving and coupling of the modes to separate baths. The presence of the latter is needed for a consistent quantum description of the dynamics based on the non-Hermitian Hamiltonian $\hat{H}(\varepsilon)$. Using input–output theory, a signal is extracted from the linear system [Eq. (24)] for which an upper bound of the signal-to-noise ratio (or the measurement rate) is derived.

The upper bound in Ref. [90] for reciprocal systems is independent of whether the sensor is at an EP or not. The conclusion reached is that EP-based sensors do not have an advantage in terms of quantum-limited signal-to-noise ratio. The derived bound is, however, not valid for non-reciprocal

systems. The authors of Ref. [90] therefore promote nonreciprocity as a resource for sensing. In contrast, the authors in Ref. [91] have concluded that EP-based sensing has a more favorable bound in the quantum regime when using an EP-based amplifier near its lasing threshold. However, their analysis is based on a linearization that might be problematic due to large fluctuations near the EP, as conjectured in Ref. [92].

The first experiment observing quantum limits of EP-based sensors was done by Wang and coworkers [94]. It is an extension of their work on Brillouin laser gyroscopes [81]; remember the discussion in Section 4 and Fig. 3(f). In strong contrast to the just-discussed theoretical approaches, the experiment went well beyond the weak dispersive limit. The key observation is that the diverging frequency-splitting enhancement of the gyroscope is precisely compensated by a diverging broadening of the laser linewidths; see Fig. 5. The origin of the latter is excess quantum noise due to the nonorthogonality of the modes. The linewidth broadening factor is called Petermann factor [95–98]. Near the EP, the nonorthogonality of the involved modes becomes extreme and the Petermann factor is therefore expected to diverge at the EP [99], even though it is difficult to imagine that this can be observed directly in an experiment. The experiment and theoretical analysis of Wang *et al.* have shown that the quantum-limited signal-to-noise ratio is not improved for EP-based sensors, at least in this kind of system.

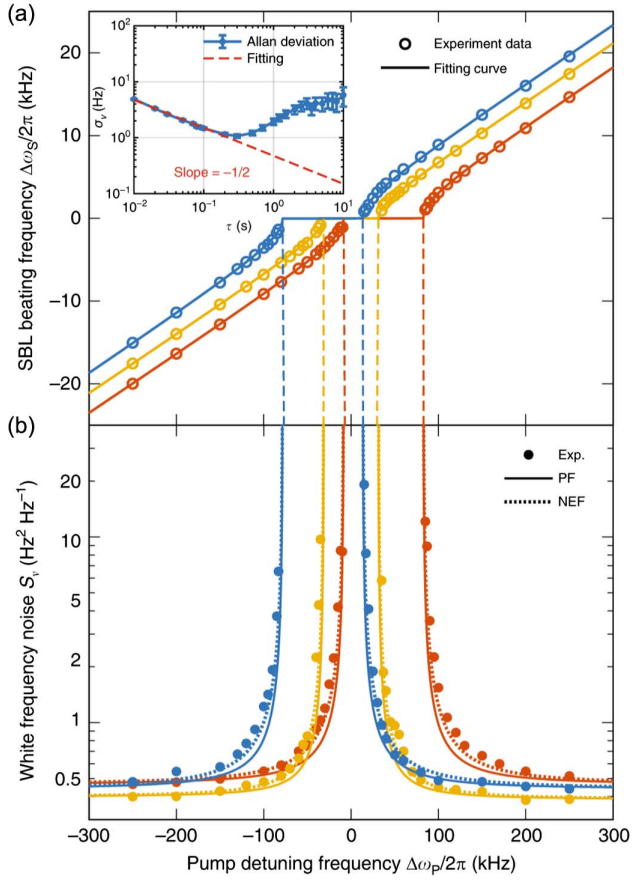

Fig. 5. Fundamental limit of an EP-based laser gyroscope due to excess quantum noise [94]. (a) Measured stimulated Brillouin laser (SBL) beating frequency versus pump detuning (which determines the frequency detuning of the uncoupled SBL modes) for different locking zones. The inset shows an Allan deviation measurement of frequency σ_ν versus gate time τ. (b) Measured white frequency noise of the beating signal determined using the Allan deviation measurement. The linewidth enhancement factor [Petermann factor (PF), solid curves] and the noise enhancement factor (NEF, dashed curves) are theoretical predictions. The figure is taken from Ref. [94].

6. SUMMARY AND OUTLOOK

I have reviewed the progress on exceptional point-based sensors since the proposal of this concept in 2014 [29]. Such a sensor exploits the enhanced response of the energy eigenvalues (frequencies) at an exceptional-point singularity on external perturbations. Several theoretical studies have broadened the field of possible applications. Eight proof-of-principle experiments have already demonstrated the potential of such sensors for particle detection, thermal sensing, thermal mapping, wireless sensing, and rotation sensing.

The deleterious influence of classical and quantum noise has been discussed. Classical noise can lead to a dynamical instability of exceptional point-based sensors operating at or close to the real frequency axis, which in turn can spoil the resolvability via the necessary stabilization [88]. The fundamental limitations due to quantum noise are still under debate. The experiment by Wang *et al.* has revealed that for laser gyroscopes, the enhanced splitting is compensated by laser linewidth broadening due to excess quantum noise [94].

For the future it would be important to have a deeper theoretical understanding of nonlinear processes in exceptional point-based sensors such as gain saturation and laser dynamics; a first step has been done in (the supplementary material of) Ref. [80]. This understanding will lead to further improvements of the performance of sensors based on exceptional points.

While the even more enhanced frequency splittings of third-order exceptional points have already been experimentally demonstrated [74], it remains to fabricate sensors with exceptional points of even higher order. This is obviously a challenging task because of the extreme sensitivity to fabrication tolerances. A promising approach to overcoming this problem is the concept of exceptional surfaces [70].

Even though most of the applications of exceptional point-based sensors will be in the classical domain, it can be expected that recent and future developments in the study of exceptional point physics in the quantum domain, see for example Refs. [89,100], will broaden the range of potential applications of exceptional point-based sensors.

Acknowledgment. I thank J. Kullig for discussions.

Disclosures. The author declares no conflicts of interest.

REFERENCES

1. W. P. Reinhardt, "Complex coordinates in the theory of atomic and molecular structure and dynamics," Ann. Rev. Phys. Chem. **33**, 223–255 (1982).
2. C. Keller, M. K. Oberthaler, R. Abfalterer, S. Bernet, J. Schmiedmayer, and A. Zeilinger, "Tailored complex potentials and

Friedel's law in atom optics," Phys. Rev. Lett. **79**, 3327–3330 (1997).
3. M. V. Berry and D. H. J. O'Dell, "Diffraction by volume gratings with imaginary potentials," J. Phys. A **31**, 2093–2101 (1998).
4. G. L. Celardo and L. Kaplan, "Superradiance transition in one-dimensional nanostructures: an effective non-Hermitian Hamiltonian formalism," Phys. Rev. B **79**, 155108 (2009).
5. G. E. Mitchell, A. Richter, and H. A. Weidenmüller, "Random matrices and chaos in nuclear physics: nuclear reactions," Rev. Mod. Phys. **82**, 2845–2901 (2010).
6. Y.-K. Lu, P. Peng, Q.-T. Cao, D. Xu, J. Wiersig, Q. Gong, and Y.-F. Xiao, "Spontaneous T-symmetry breaking and exceptional points in cavity quantum electrodynamics systems," Sci. Bull. **63**, 1096–1100 (2018).
7. H.-J. Stöckmann, E. Persson, Y.-H. Kim, M. Barth, U. Kuhl, and I. Rotter, "Effective Hamiltonian for a microwave billiard with attached waveguide," Phys. Rev. E **65**, 066211 (2002).
8. C. E. Rüter, K. G. Makris, R. El-Ganainy, D. N. Christodoulides, M. Segev, and D. Kip, "Observation of parity-time symmetry in optics," Nat. Phys. **6**, 192–195 (2010).
9. J. Wiersig, "Structure of whispering-gallery modes in optical microdisks perturbed by nanoparticles," Phys. Rev. A **84**, 063828 (2011).
10. C. M. Bender and S. Boettcher, "Real spectra in non-Hermitian Hamiltonians having PT symmetry," Phys. Rev. Lett. **80**, 5243–5246 (1998).
11. A. Regensburger, C. Bersch, M.-A. Miri, G. Onishchukov, D. N. Christodoulides, and U. Peschel, "Parity-time synthetic photonic lattices," Nature **488**, 167–171 (2012).
12. B. Peng, Ş. K. Özdemir, F. Lei, F. Monfi, M. Gianfreda, G. L. Long, S. Fan, F. Nori, C. M. Bender, and L. Yang, "Parity-time-symmetric whispering-gallery microcavities," Nat. Phys. **10**, 394–398 (2014).
13. S. Scheel and A. Szameit, "PT-symmetric photonic quantum systems with gain and loss do not exit," Eur. Phys. Lett. **122**, 34001 (2018).
14. R. El-Ganainy, K. G. Makris, M. Khajavikhan, Z. H. Musslimani, and D. N. Christodoulides, "Non-Hermitian physics and PT symmetry," Nat. Phys. **14**, 11–19 (2018).
15. L. Feng, R. El-Ganainy, and L. Ge, "Non-Hermitian photonics based on parity-time symmetry," Nat. Photonics **11**, 752–762 (2017).
16. T. Kato, *Perturbation Theory for Linear Operators* (Springer, 1966).
17. W. D. Heiss, "Repulsion of resonance states and exceptional points," Phys. Rev. E **61**, 929–932 (2000).
18. M. V. Berry, "Physics of nonhermitian degeneracies," Czech. J. Phys. **54**, 1039–1047 (2004).
19. W. D. Heiss, "Exceptional points of non-Hermitian operators," J. Phys. A **37**, 2455–2464 (2004).
20. C. Dembowski, H.-D. Gräf, H. L. Harney, A. Heine, W. D. Heiss, H. Rehfeld, and A. Richter, "Experimental observation of the topological structure of exceptional points," Phys. Rev. Lett. **86**, 787–790 (2001).
21. C. Dembowski, B. Dietz, H.-D. Gräf, H. L. Harney, A. Heine, W. D. Heiss, and A. Richter, "Encircling an exceptional point," Phys. Rev. E **69**, 056216 (2004).
22. B. Dietz, T. Friedrich, J. Metz, M. Miski-Oglu, A. Richter, F. Schäfer, and C. A. Stafford, "Rabi oscillations at exceptional points in microwave billiards," Phys. Rev. E **75**, 027201 (2007).
23. S.-B. Lee, J. Yang, S. Moon, S.-Y. Lee, J.-B. Shim, S. W. Kim, J.-H. Lee, and K. An, "Observation of an exceptional point in a chaotic optical microcavity," Phys. Rev. Lett. **103**, 134101 (2009).
24. J. Zhu, Ş. K. Özdemir, L. He, and L. Yang, "Controlled manipulation of mode splitting in an optical microcavity by two Rayleigh scatterers," Opt. Express **18**, 23535–23543 (2010).
25. B. Peng, Ş. K. Özdemir, M. Liertzer, W. Chen, J. Kramer, H. Yilmaz, J. Wiersig, S. Rotter, and L. Yang, "Chiral modes and directional lasing at exceptional points," Proc. Natl. Acad. Sci. USA **113**, 6845–6850 (2016).
26. S. Richter, H.-G. Zirnstein, J. Zúñiga-Pérez, E. Krüger, C. Deparis, L. Trefflich, C. Sturm, B. Rosenow, M. Grundmann, and R. Schmidt-Grund, "Voigt exceptional points in an anisotropic ZnO-based planar microcavity: square-root topology, polarization vortices, and circularity," Phys. Rev. Lett. **123**, 227401 (2019).
27. M.-A. Miri and A. Alù, "Exceptional points in optics and photonics," Science **363**, eaar7709 (2019).
28. Ş. K. Özdemir, S. Rotter, F. Nori, and L. Yang, "Parity-time symmetry and exceptional points in photonics," Nat. Mater. **18**, 783–798 (2019).
29. J. Wiersig, "Enhancing the sensitivity of frequency and energy splitting detection by using exceptional points: application to microcavity sensors for single-particle detection," Phys. Rev. Lett. **112**, 203901 (2014).
30. J. Zhu, Ş. K. Özdemir, Y.-F. Xiao, L. Li, L. He, D.-R. Chen, and L. Yang, "On-chip single nanoparticle detection and sizing by mode splitting in an ultrahigh-Q microresonator," Nat. Photonics **4**, 46–49 (2010).
31. L. He, Ş. K. Özdemir, J. Zhu, W. Kim, and L. Yang, "Detecting single viruses and nanoparticles using whispering gallery microlasers," Nat. Nanotechnol. **6**, 428–432 (2011).
32. F. Vollmer and L. Yang, "Label-free detection with high-Q microcavities: a review of biosensing mechanisms for integrated devices," Nanophotonics **1**, 267–291 (2012).
33. W. W. Chow, J. Gea-Banacloche, L. M. Pedrotti, V. E. Sanders, W. Schleich, and M. O. Scully, "The ring laser gyro," Rev. Mod. Phys. **57**, 61–104 (1985).
34. S. Sunada and T. Harayama, "Design of resonant microcavities: application to optical gyroscopes," Opt. Express **15**, 16245–16254 (2007).
35. L. Rondin, J.-P. Tetienne, T. Hingant, J.-F. Roch, P. Maletinsky, and V. Jacques, "Magnetometry with nitrogen-vacancy defects in diamond," Rep. Prog. Phys. **77**, 056503 (2014).
36. E. Gil-Santos, D. Ramos, J. Martínez, M. Fernández-Regúlez, R. García, A. San Paulo, M. Calleja, and J. Tamayo, "Nanomechanical mass sensing and stiffness spectrometry based on two-dimensional vibrations of resonant nanowires," Nat. Nanotechnol. **5**, 641–645 (2010).
37. Y. Liu, L. Zhang, J. A. R. Williams, and I. Bennio, "Optical bend sensor based on measurement of resonance mode splitting of long-period fiber grating," IEEE Photon. Technol. Lett. **12**, 531–533 (2000).
38. J. Wiersig, "Sensors operating at exceptional points: general theory," Phys. Rev. A **93**, 033809 (2016).
39. J. Wiersig, "Non-Hermitian effects due to asymmetric backscattering of light in whispering-gallery microcavities," in *Parity-time Symmetry and Its Applications*, D. Christodoulides and J. Yang, eds. (Springer, 2018), pp. 155–184.
40. A. Mazzei, S. Götzinger, L. de S. Menezes, G. Zumofen, O. Benson, and V. Sandoghdar, "Controlled coupling of counterpropagating whispering-gallery modes by a single Rayleigh scatterer: a classical problem in a quantum optical light," Phys. Rev. Lett. **99**, 173603 (2007).
41. J. Wiersig, "Nonorthogonality constraints in open quantum and wave systems," Phys. Rev. Res. **1**, 033182 (2019).
42. L. He, Ş. K. Özdemir, J. Zhu, and L. Yang, "Ultrasensitive detection of mode splitting in active optical microcavities," Phys. Rev. A **82**, 053810 (2010).
43. J. Knittel, T. G. McRae, K. H. Lee, and W. P. Bowen, "Interferometric detection of mode splitting for whispering-gallery mode biosensors," Appl. Phys. Lett. **97**, 123704 (2010).
44. U. Kuhl, R. Höhmann, J. Main, and H.-J. Stöckmann, "Resonance widths in open microwave cavities studied by harmonic inversion," Phys. Rev. Lett. **100**, 254101 (2008).
45. W. Langbein, "No exceptional precision of exceptional-point sensors," Phys. Rev. A **98**, 023805 (2018).
46. K. J. Vahala, "Optical microcavities," Nature **424**, 839–846 (2003).
47. H. Cao and J. Wiersig, "Dielectric microcavities: model systems for wave chaos and non-Hermitian physics," Rev. Mod. Phys. **87**, 61–111 (2015).
48. L. Shao, X.-F. Jiang, X.-C. Yu, B.-B. Li, W. R. Clements, F. Vollmer, W. Wang, Y.-F. Xiao, and Q. Gong, "Detection of single nanoparticles and lentiviruses using microcavity resonance broadening," Adv. Mater. **25**, 5616–5620 (2013).

49. J. Wiersig, S. W. Kim, and M. Hentschel, "Asymmetric scattering and nonorthogonal mode patterns in optical microspirals," Phys. Rev. A **78**, 053809 (2008).
50. J. Wiersig, A. Eberspächer, J.-B. Shim, J.-W. Ryu, S. Shinohara, M. Hentschel, and H. Schomerus, "Nonorthogonal pairs of copropagating optical modes in deformed microdisk cavities," Phys. Rev. A **84**, 023845 (2011).
51. J. Wiersig, "Chiral and nonorthogonal eigenstate pairs in open quantum systems with weak backscattering between counterpropagating traveling waves," Phys. Rev. A **89**, 012119 (2014).
52. S. Liu, J. Wiersig, W. Sun, Y. Fan, L. Ge, J. Yang, S. Xiao, Q. Song, and H. Cao, "Transporting the optical chirality through the dynamical barriers in optical microcavities," Laser Photon. Rev. **12**, 1800027 (2018).
53. W. D. Heiss and H. L. Harney, "The chirality of exceptional points," Eur. Phys. J. D **17**, 149–151 (2001).
54. C. Dembowski, B. Dietz, H.-D. Gräf, H. L. Harney, A. Heine, W. D. Heiss, and A. Richter, "Observation of a chiral state in a microwave cavity," Phys. Rev. Lett. **90**, 034101 (2003).
55. C. Wang, X. Jiang, G. Zhao, M. Zhang, C. W. Hsu, B. Peng, A. D. Stone, and L. Yang, "Electromagnetically induced transparency at a chiral exceptional point," Nat. Phys. **16**, 334–340 (2020).
56. J. Kullig and J. Wiersig, "High-order exceptional points of counterpropagating waves in weakly deformed microdisk cavities," Phys. Rev. A **100**, 043837 (2019).
57. J. Kullig, M. Yi, C.-H. Hentschel, and J. Wiersig, "Exceptional points of third-order in a layered optical microdisk cavity," New J. Phys. **20**, 083016 (2018).
58. A. Hassan, H. Hodaei, W. Hayenga, M. Khajavikhan, and D. Christodoulides, "Enhanced sensitivity in parity-time-symmetric microcavity sensors," in *Advanced Photonics*, OSA Technical Digest (online) (Optical Society of America, 2015), paper SeT4C.3.
59. W. Chen, J. Zhang, B. Peng, Ş. K. Özdemir, X. Fan, and L. Yang, "Parity-time-symmetric whispering-gallery mode nanoparticle sensor," Photon. Res. **6**, A23–A30 (2018).
60. S. Zhang, Z. Yong, Y. Zhang, and S. He, "Parity-time symmetry breaking in coupled nanobeam cavities," Sci. Rep. **6**, 24487 (2015).
61. Z.-P. Liu, J. Zhang, Ş. K. Özdemir, B. Peng, H. Jing, X.-Y. Lü, C.-W. Li, L. Yang, F. Nori, and Y.-X. Liu, "Metrology with PT-symmetric cavities: enhanced sensitivity near the PT-phase transition," Phys. Rev. Lett. **117**, 110802 (2016).
62. J. Ren, H. Hodaei, G. Harari, A. U. Hassan, W. Chow, M. Soltani, D. Christodoulides, and M. Khajavikhan, "Ultrasensitive micro-scale parity-time-symmetric ring laser gyroscope," Opt. Lett. **42**, 1556–1559 (2017).
63. S. Sunada, "Large Sagnac frequency splitting in a ring resonator operating at an exceptional point," Phys. Rev. A **96**, 033842 (2017).
64. R. Sarma, L. Ge, J. Wiersig, and H. Cao, "Rotating optical microcavities with broken chiral symmetry," Phys. Rev. Lett. **114**, 053903 (2015).
65. B. Jin, W. Tan, C. Zhang, J. Wu, J. Chen, S. Zhang, and P. Wu, "High-performance terahertz sensing at exceptional points in a bilayer structure," Adv. Theory Simul. **1**, 1800070 (2018).
66. A. Jian, F. Liu, G. Bai, B. Zhang, Y. Zhang, Q. Zhang, X. Xue, S. Sang, and X. Zhang, "Parity-time symmetry based on resonant optical tunneling effect for biosensing," Opt. Commun. **475**, 125815 (2020).
67. M. Goryachev, B. McAllister, and M. E. Tobar, "Probing dark universe with exceptional points," Phys. Dark Univ. **23**, 100244 (2018).
68. J. Liu, L. Chen, and K.-D. Zhu, "Enhanced sensing of non-Newtonian effects at ultrashort range with exceptional points in optomechanical systems," arXiv:191205732 (2019).
69. J. Liu, L. Chen, F. He, and K.-D. Zhu, "Gravitational waves detection with exceptional points in micro cavities," arXiv:2001.09462 (2019).
70. Q. Zhong, J. Ren, M. Khajavikhan, D. N. Christodoulides, Ş. K. Özdemir, and R. El-Ganainy, "Sensing with exceptional surfaces in order to combine sensitivity with robustness," Phys. Rev. Lett. **122**, 153902 (2019).
71. Q. Zhong, S. Nelson, Ş. K. Özdemir, and R. El-Ganainy, "Controlling direction absorption with chiral exceptional surfaces," Opt. Lett. **44**, 5242–5245 (2019).
72. S. Wang, B. Hou, W. Lu, Y. Chen, Z. Q. Zhang, and C. T. Chan, "Arbitrary order exceptional point induced by photonic spin-orbit interaction in coupled resonators," Nat. Commun. **10**, 832 (2019).
73. W. Chen, Ş. K. Özdemir, G. Zhao, J. Wiersig, and L. Yang, "Exceptional points enhance sensing in an optical microcavity," Nature **548**, 192–196 (2017).
74. H. Hodaei, A. Hassan, S. Wittek, H. Carcia-Cracia, R. El-Ganainy, D. Christodoulides, and M. Khajavikhan, "Enhanced sensitivity at higher-order exceptional points," Nature **548**, 187–191 (2017).
75. H. Zhao, Z. Chen, R. Zhao, and L. Feng, "Exceptional points engineered glass slide for microscopic thermal mapping," Nat. Commun. **9**, 1764 (2018).
76. M. Sakhdari, M. Hajizadegan, Y. Li, M. M.-C. Cheng, J. C. H. Hung, and P.-Y. Chen, "Ultrasensitive, parity-time-symmetric wireless reactive and resistive sensors," IEEE Sens. J. **18**, 9548–9555 (2018).
77. P.-Y. Chen, M. Sakhdari, M. Hajizadegan, Q. Cui, M. M.-C. Cheng, R. El-Ganainy, and A. Alù, "Generalized parity-time symmetry condition for enhanced sensor telemetry," Nat. Electron. **1**, 297–304 (2018).
78. Z. Dong, Z. Li, F. Yang, C.-W. Qiu, and J. S. Ho, "Sensitive readout of implantable microsensors using a wireless system locked to an exceptional point," Nat. Electron. **2**, 335–342 (2019).
79. C. Zeng, Y. Sun, G. Li, Y. Li, H. Jiang, Y. Yang, and H. Chen, "Enhanced sensitivity at high-order exceptional points in a passive wireless sensing system," Opt. Express **27**, 27562–27572 (2019).
80. M. P. Hokmabadi, A. Schumer, D. N. Christodoulides, and M. Khajavikhan, "Non-Hermitian ring laser gyroscopes with enhanced Sagnac sensitivity," Nature **576**, 70–74 (2019).
81. Y.-H. Lai, Y.-K. Lu, M.-G. Suh, Z. Yuan, and K. Vahala, "Observation of the exceptional-point-enhanced Sagnac effect," Nature **576**, 65–69 (2019).
82. J. Miller, "Exceptional points make for exceptional sensors," Phys. Today **70**, 23–26 (2017).
83. L. Ge, Y. D. Chong, and A. D. Stone, "Conservation relations and anisotropic transmission resonances in one-dimensional PT-symmetric photonic heterostructures," Phys. Rev. A **85**, 023802 (2012).
84. J.-H. Park, A. Ndao, L. Hsu, A. Kodigala, T. Lepetit, Y.-H. Lo, and B. Kanté, "Symmetry-breaking-induced plasmonic exceptional points and nanoscale sensing," Nat. Phys. **16**, 462–468 (2020).
85. N. A. Mortensen, P. A. D. Gonçalves, M. Khajavikhan, D. N. Christodoulides, C. Tserkezis, and C. Wolff, "Fluctuations and noise-limited sensing near the exceptional point of parity-time-symmetric resonator systems," Optica **5**, 1342–1346 (2018).
86. C. Wolff, C. Tserkezis, and N. A. Mortensen, "On the time evolution at a fluctuating exceptional point," Nanophotonics **8**, 1319–1326 (2019).
87. Z. Xiao, H. Li, T. Kottos, and A. Alù, "Enhanced sensing and nondegraded thermal noise performance based on PT-symmetric electronic circuits with a sixth-order exceptional point," Phys. Rev. Lett. **123**, 213901 (2019).
88. J. Wiersig, "Robustness of exceptional-point-based sensors against parametric noise: the role of Hamiltonian and Liouvillian degeneracies," Phys. Rev. A **101**, 053846 (2020).
89. F. Minganti, A. Miranowicz, R. W. Chhajlany, and F. Nori, "Quantum exceptional points of non-Hermitian Hamiltonians and Liouvillians: the effects of quantum jumps," Phys. Rev. A **100**, 062131 (2019).
90. H.-K. Lau and A. A. Clerk, "Fundamental limits and non-reciprocal approaches in non-Hermitian quantum sensing," Nat. Commun. **9**, 4320 (2018).
91. M. Zhang, W. Sweeney, C. W. Hsu, L. Yang, A. D. Stone, and L. Jiang, "Quantum noise theory of exceptional point amplifying sensors," Phys. Rev. Lett. **123**, 180501 (2019).
92. C. Chen, L. Jin, and R.-B. Liu, "Sensitivity of parameter estimation near the exceptional point of a non-Hermitian system," New J. Phys. **21**, 083002 (2019).
93. S. Sunada, "Enhanced response of non-Hermitian photonic systems near exceptional points," Phys. Rev. A **97**, 043804 (2018).
94. H. Wang, Y.-H. Lai, Z. Yuan, M.-G. Suh, and K. Vahala, "Petermann-factor sensitivity limit near an exceptional point in a Brillouin ring laser gyroscope," Nat. Commun. **11**, 1610 (2020).

95. K. Petermann, "Calculated spontaneous emission factor for double-heterostructure injection lasers with gain-induced waveguiding," IEEE J. Quantum Electron. **15**, 566–570 (1979).
96. A. E. Siegman, "Excess spontaneous emission in non-Hermitian optical systems. I. Laser amplifiers," Phys. Rev. A **39**, 1253–1263 (1989).
97. A. E. Siegman, "Excess spontaneous emission in non-Hermitian optical systems. II. Laser oscillators," Phys. Rev. A **39**, 1264–1268 (1989).
98. H. Schomerus, "Excess quantum noise due to mode orthogonality in dielectric microresonators," Phys. Rev. A **79**, 061801 (2009).
99. M. V. Berry, "Mode degeneracies and the Petermann excess-noise factor for unstable lasers," J. Mod. Opt. **50**, 63–81 (2003).
100. M. Naghiloo, M. Abbasi, Y. N. Joglekar, and K. W. Murch, "Quantum state tomography across the exceptional point in a single dissipative qubit," Nat. Phys. **15**, 1232–1236 (2019).